

# Sugar-Ester Nonionic Microemulsion: Structural Characterization

Otto Glatter,<sup>\*,1</sup> Doris Orthaber,<sup>\*</sup> Anna Stradner,<sup>\*</sup> Günther Scherf,<sup>\*</sup> Monzer Fanun,<sup>†</sup> Nissim Garti,<sup>‡</sup>  
Véronique Clément,<sup>‡</sup> and Martin E. Leser<sup>‡</sup>

<sup>\*</sup>Institute of Chemistry, Physical Chemistry, University of Graz, Graz A-8010, Austria; <sup>†</sup>Casali Institute, Hebrew University of Jerusalem, IL-91904 Jerusalem, Israel; and <sup>‡</sup>Nestlé Research Center, CH-1000 Lausanne 26, Switzerland

E-mail: otto.glatter@uni-graz.at

Received November 21, 2000; accepted April 30, 2001; published online July 25, 2001

Surfactants containing sugar components and fatty acids satisfy the quality standards for food application. The food grade sugar ester in this study is a commercial sucrose monoester of stearic acid (abbreviated SES), the oil phase consists of a 1:1 mixture of *n*-tetradecane and *l*-butanol. The originally planned food grade oil, a medium chain triglyceride, is substituted by tetradecane because tetradecane is available as a fully deuterated product, which is necessary for some structural investigations. The investigated system is solid at room temperature, but liquefies and structures into a homogeneous microemulsion when heated to above 37°C. The structural characterization of such microemulsions is the aim of this work. The established methods for this purpose are scattering methods, such as small-angle scattering of X-rays and neutrons and dynamic light scattering. These scattering techniques can be used to obtain valuable information on the size, shape, and internal structure of colloids and complex fluids. We started our investigation with the pseudobinary system SES, tetradecane and *l*-butanol, varying the SES content. The scattering results show that the sugar ester form inverse globular micelles in the oil phase. The size of these micelles is about 6 nm. While the size is nearly constant in a wide SES concentration regime (5 up to 40% surfactant), the volume or aggregation number increases significantly with SES. This is explained by an increasing replacement of *l*-butanol molecules by sugar-ester molecules in the micelles formed. Moreover, it can be shown that these micelles strongly overlap. Their center-to-center distance is about 3.8 nm at 40% SES at a micellar diameter of 6 nm. The micellar overlap leads to a highly reduced diffusion of the micelles as was found with dynamic light scattering. When incorporating water in the micellar core, the micelles swell up to about 10 nm and the shape of the aggregates becomes more and more elongated with higher water content. © 2001 Academic Press

**Key Words:** sugar surfactant; microemulsions; structural investigations; dynamic light scattering; small angle X-ray scattering; small angle neutron scattering.

## I. INTRODUCTION

Microemulsions are isotropic and thermodynamically stable solutions, in which two immiscible liquids, i.e., water and oil,

are brought together by means of an appropriate surfactant or surfactant/co-surfactant mixture (1). The used surfactants can be either charged (ionic surfactants) or uncharged (nonionic surfactants). Microemulsions, based on nonionic surfactants, have been extensively investigated, both from a formulation, i.e. phase behavior, and a structural point of view (1–7). In almost all nonionic microemulsions the nonionic surfactants used are ethoxylated surfactants, such as ethoxylated alcohols, acids and fats, monoglycerides, and sorbitan esters. However, only a limited amount of work was conducted on the polyol type of nonionic surfactants, such as glucoside ethers or sucrose esters of fatty acids (8–10). These surfactants are biodegradable and formed from renewable sources such as fatty acids and sugars. They can be manufactured with various HLB values (hydrophilic lipophilic balance), which provide various hydrophilic lipophilic properties. The cosmetic industry is well aware of the possibilities arising from the use of sucrose esters for the preparation of nonionic microemulsions (9). For food science, however, such microemulsions are in the starting phase of investigations. These systems can have advantages in applications such as toppings or coatings of food products.

The physical properties of sucrose esters are somewhat unique. Unlike the alkyl ethoxylates, the sucrose esters do not significantly change their HLB with increasing temperature. Consequently, increasing the temperature does not induce a phase inversion in microemulsion systems based on sucrose esters, as was observed in microemulsions based on alkyl ethoxylates. Temperature-insensitive sucrose-ester-based microemulsions are described in the literature (8, 11, 12). In most cases a paraffinic oil phase was used and the surfactants were mostly mixtures of ethoxylated alcohols and sucrose esters.

Kawaguchi *et al.* (13) studied the micellar structure (direct micelles) of a homologous series of the fatty acid sucrose monoesters,  $C_nSE$  ( $n = 10, 12, 14, 16$ ) by X-ray scattering techniques. Parameters such as  $R_v$ , maximum dimension of the micelles, were calculated, and from the 150 scattering points they deduced that the micelles are not spherical. Other parameters such as aggregation number and hydration ratio were also obtained. It was concluded that the micellar shape was oblate for

<sup>1</sup> To whom correspondence should be addressed. Fax: +43 316 380 9850.

C<sub>10</sub>SE, C<sub>12</sub>SE, and C<sub>14</sub>SE but prolate for C<sub>16</sub>SE. X-ray scattering curves show the possibility that both types of ellipsoid coexist in the solution of C<sub>16</sub>SE at 20°C. The polydispersity in micellar size was found to be small.

Since the most common sucrose esters are hydrophilic it was not expected that these surfactants will form reverse micelles or w/o microemulsions. However, recently, Garti *et al.* (14) showed that the addition of a cosolvent/coemulsifier, such as short- or medium-chain alcohols, induces the formation of reverse micelles and the solubilization of significant amounts of water into the micellar core to form water-in-oil microemulsions. Up to 60% of water could be solubilized in a system consisting of sucrose monoester of stearic acid/propanol/ MCT (medium-chain triglyceride) at a weight ratio of 1/3/1 (14).

Only limited work dealing with the investigation of the microstructure formed in sucrose-ester-based w/o microemulsions has been done so far. Bolzinger-Thevenin *et al.* (10) attempted to characterize the single-phase region (Winsor IV) of systems consisting of sucrose monolaurate and sucrose dilaurate, diethylene glycol monoethyl ether, water, and alkyl esters as the oil at fixed surfactant + cosurfactant/oil weight ratio of 40/60. The microstructure has been probed along a single water dilution line using freeze fracture electron microscopy and small-angle neutron scattering. In this dilution line, up to 40 wt% water can be solubilized. The authors postulated that the microemulsion mixture along this path (20 to 45 wt% water) has a bicontinuous microstructure. The system behaves quite particularly and does not reflect a behavior of classical water-in-oil microemulsions. The authors did not study the ternary mixtures of oil + surfactant + cosurfactant and did not explore in detail the areas of low amounts of solubilized water. The paper is aimed mainly to demonstrate the existence of bicontinuous areas.

Recently, Garti *et al.* (14) and Fanun *et al.* (15) also measured quite particular features in another sucrose-ester-based w/o microemulsion: While in nonionic alkyl ethoxylate-based w/o microemulsions the viscosity increases with increasing water content in the system, in the sucrose monostearate-based system the viscosity decreases with increasing water content. Moreover, the electrical conductivity increases only slightly as a function of the water content and does not show the typical bicontinuous percolation behavior.

In the present work, the structural properties of w/o sucrose-ester microemulsions will be investigated in more detail by means of SAXS (small-angle X-ray scattering), SANS (small-angle neutron scattering), and DLS (dynamic light scattering). These scattering techniques can be used to obtain valuable information on size, shape, internal structure, and diffusion dynamics of colloids and complex fluids. Especially their use for the characterization of self-organizing amphiphilic systems like microemulsions has proven to be very effective (16).

The sugar ester used is a commercial sucrose monoester of stearic acid (S-1570, denoted as SES, HLB = 15, at least 70% monoester) in a mixture with di- and polyesters of stearic and palmitic acids. The oil phase consists of a 1:1 mixture of tetradecane and 1-butanol.

The addition of the cosolvent (1-butanol) to the oil phase turned the oil phase into a better solvent and allowed significant solubilization of the surfactant into the oil with the formation of inverse micelles. The cosolvent is necessary because of the hydrophilicity of the sucrose monostearate and hydrophobicity of the oil. It should be mentioned that 1-butanol is added to the oil phase. However, due to its amphiphilic character it will redistribute also into the interface and must therefore be considered also as a cosurfactant and not just as a cooil; i.e., it has the ability to participate in the self-assembly with the surfactant.

The originally planned food grade oil, a medium-chain triglyceride (MCT, Migliol 818), is substituted by tetradecane because tetradecane is available as a fully deuterated product, which is necessary for SANS investigations.

The microemulsion system used is solid at room temperature, but liquefies and structures into a homogeneous microemulsion when heated above 37°C. The solid-liquid transformations at high water solubilization fraction, together with heat resistance properties, make it possible to immobilize water soluble materials and preserve activity or stability of active matters such as enzymes, aroma molecules, and volatile oxidation-sensitive compounds. The solid-liquid transition is an important feature in using microemulsions as microreactors.

The problems for the use of these model systems for food grade microemulsions are: (1) cosurfactants (alcohols) are necessary to make microemulsions with sucrose esters, (2) there are low availability and high costs of sucrose esters, (3) sugar esters are not approved for use in foods in many countries, and (4) there is a lack of sufficient characterization and purification since most commercial sucrose esters are complex mixtures of mono-, di, and polyesters of mixed fatty acids. Therefore one important step to overcome some of these disadvantages is the structural characterization of such microemulsions, which is the aim of this work. We started our investigation with the pseudobinary system (SES in the mixture of tetradecane/1-butanol, i.e., no water present) and studied the structural evolution as a function of the sucrose-ester content. Then we analyzed the structural evolution as a function of the water content, keeping the ratio of sucrose ester to (tetradecane + butanol) constant at 40/60.

## II. MATERIALS AND SAMPLE PREPARATION

The food grade sucrose monostearate S-1570 (in the following denoted as SES) was received from Mitsubishi-Kagaku Food Corp. The other reagents used were purchased in the highest obtainable grade from Merck (1-butanol, D<sub>2</sub>O) or Aldrich (tetradecane). The deuterated tetradecane and 1-butanol were received from CDN isotopes; the tetradecane was deuterated to 98% and the 1-butanol to 99.5%. The solvents for the neutron measurements were deuterated (tetradecane, 1-butanol, and water) and for the X-ray measurements protonated. Deuterated chemicals were needed for the SANS experiments in order to reduce the incoherent scattering and to have increased contrast. The

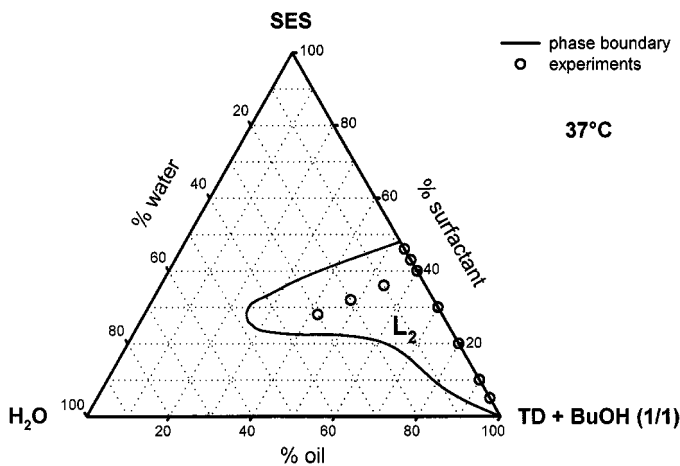


**FIG. 1.** Phase diagram for the four-component system at 37°C containing SES (sucrose monoester S-1570), tetradecane/1-butanol, and water. The  $L_2$  region shows the microemulsion region, and the circles mark the experimental compositions.

coherent scattering length densities for the chemicals used are 653.1 for *d*-butanol, 681.3 for *d*-tetradecane, 638.2 for  $D_2O$ , and 63.3 for SES (all values are in units of  $10^{-10} \text{ cm}^{-2}$ ).

All compounds are chemically pure and used without further purification. The samples are prepared, equilibrated for at least 24 h, and measured at 37°C. Throughout, the concentrations are given in weight percent (wt%). The quality of the samples is routinely examined with dynamic light scattering. The phase behavior of the system (see Fig. 1) did not change when using deuterated chemicals. All experimental compositions were in the clear one-phase regime  $L_2$ . We did not check for small changes in the boundaries of the  $L_2$  phase due to the high price of the deuterated substances. The region that adjoins to the one-phase  $L_2$  regime is a coexistence of excess water and the  $L_2$  phase.

### III. METHODS

#### *Small-Angle Scattering (SAS)*

SAS, in particular, SANS and SAXS, probe the pertinent colloidal length scales of 1–100 nm and therefore are the methods of choice for determining the size, shape, and internal structure of colloidal particles. In addition, because the two kinds of scattered radiation are sensitive to different physical properties of the scattering particle, these techniques can be used in parallel to obtain a rich variety of information. The scattering intensity depends on the different scattering length densities of the particles and the solvent. The scattering length is a complex function of the atomic number for SANS and must be determined experimentally. For SAXS the scattering length density is proportional to the electron density, which is a linear function of the number of electrons. Consequently, SAXS is particularly useful for investigating the interfacial region of aggregates composed of surfactant molecules (17). However, at the time of these exper-

iments, SAXS data were not measured on absolute scale and so all data are presented in arbitrary units.

SANS and SAXS were used to obtain information on the size of the micelles and on their internal structure. Only the polar headgroups and water regions are visible with SAXS experiments due to the fact that their electron densities are higher than the electron density of the surrounding oil. The complete protonated surfactant layer and the  $D_2O$  core is visible with SANS in deuterated oil.

The scattering curves were interpreted in real space in terms of their pair distance distribution function (PDDF) (18, 19). The PDDF  $p(r)$  is the Fourier transform of the angle-dependent scattering intensity  $I(q)$ ,  $q$  is the length of the scattering vector and is defined by  $q = (4\pi/\lambda) \sin \theta/2$ , where  $\lambda$  is the wavelength, and  $\theta$  is the scattering angle. A quantitative numerical analysis of properly pretreated data (after correction of instrumental broadening from slit smearing in the block collimation system of the Kratky camera and wavelength smearing for neutrons) involving model-independent inverse Fourier transformation provides information not available elsewhere. The PDDF represents a histogram of distances inside the particle weighted with the scattering length density differences and goes to 0 at the maximum particle dimension. So one can directly read out the diameter from this function. For globular micelles with constant contrast the PDDF is a bell-shaped function with its maximum at about half of the diameter. The area under the PDDF is proportional to the forward-scattering intensity and so to the aggregation number. In order to allow the comparison of results from different concentrations or volume fractions  $\Phi$ , the scattering data must be normalized to  $\Phi$ . Under these conditions the PDDFs are identical if there is only an increase in the number of micelles with  $\Phi$  and no change in aggregation number or shape.

The PDDF is closely related to the convolution square (spatial correlation function) of the excess scattering length density distribution  $\Delta\rho(r)$ . The radially averaged density distribution across the micelle can be obtained by deconvolution of the PDDF (20–23) assuming spherical symmetry.

The measured samples are in a concentration range where the conventional evaluation technique cannot be used. The interaction of the particles in solution must be taken into account due to the high weight fractions. In the case of interacting globular particles the scattering intensity  $I(q)$  can be written as the product of the particle form factor  $P(q)$  and the structure factor  $S(q)$ .  $S(q)$  describes the interparticle interference. For ideally diluted solutions  $S(q)$  is a constant. The scattering curves show the development of a structure factor with a pronounced maximum for increasing concentrations, superposed on the particle form factor. The evaluation of such concentrated solutions is now possible with the recently developed “generalized indirect Fourier transformation” (GIFT) (24–27). With this technique it is possible to determine simultaneously the form factor and the structure factor. This method is model free in respect to the form factor and is based on a hard sphere model for the structure factor and, strictly speaking, it is only valid for spherical,

homogeneous, and uncharged particles. However, recent applications have shown that the GIFT method can be used far beyond this theoretical limit (26), so the technique can be used for inhomogeneous, nonglobular, and polydisperse systems. It is, for instance, possible to follow sphere-to-rod transition of binary and ternary systems (26, 28). A version for charged systems is under development (29). The common feature for all these applications is the fact that the particle form factor can be determined without any model while a rather simple model is used to describe particle interactions represented by the structure factor. The typical parameters for the structure factor model are mean interaction radius, volume fraction, and polydispersity. The most important parameter that is determined in these calculations is the mean hard sphere interaction radius  $R_{HS}$ . It is half the center-to-center distance between two micelles at closest contact. The charge can be determined for ionic systems if the molarity of the salt is known. For further details the reader is referred to the original literature.

#### *Small-Angle Neutron Scattering (SANS)*

SANS measurements have been performed with the D22 instrument of the Institute Laue Langevin (ILL), France. The range of  $0.03 < q < 4.75 \text{ nm}^{-1}$  was covered for the scattering vectors by two sample-to-detector distances ( $d = 2$  and  $18 \text{ m}$ ). The neutron wavelength was  $0.6 \text{ nm}$  for all experiments. The wavelength resolution was 10% (full-width at half-maximum value). All experiments were done with a 39-cm detector offset. The samples were kept in stoppered quartz cells (Hellma, Germany) with a path length of  $1 \text{ mm}$ . The raw spectra were corrected for background from the solvent, sample cell, and electronic noise by conventional procedures. The two-dimensional scattering spectra were azimuthally averaged and corrected for detector efficiency by dividing with the incoherent scattering spectra of pure water. Data were not placed on absolute scale.

#### *Small-Angle X-ray Scattering (SAXS)*

SAXS experiments were performed using an X-ray generator M18X<sup>CE</sup> (Bruker AXS) operating at 35 kV and 250 mA with a rotating Cu anode ( $K_\alpha$  wavelength of  $0.154 \text{ nm}$ ). A Kratky compact camera (slit collimation system) was equipped with a thermostated sample holder (Anton Paar KG, Graz, Austria) and an image plate detector (Fuji BAS-1800) (30). A Göbel mirror was used as monochromator and collimator, so the  $K_\alpha$  radiation was separated from the  $K_\beta$  radiation and from the hard X-rays. Data were not placed on absolute scale and depicted in the range of  $0.102 < q \leq 5.0 \text{ nm}^{-1}$  for the scattering vectors.

#### *Dynamic Light Scattering (DLS)*

DLS measures the relaxation time of any fluctuation in refractive index occurring within the length scale defined by the scattering vector  $q$ . For  $q \times R_g \ll 1$  with  $R_g$  being the radius of gyration, the fluctuation arises from the random diffusion of the particles and the light scattered by them fluctuates in intensity.

Thus the time dependence of the scattering intensity, represented by its correlation function, provides information on the motion of the scatterer. If all particles are of the same size the correlation function is a single exponential function. Its decay is governed by the diffusion coefficient. Average hydrodynamic radii for polydisperse samples can be obtained by the method of cumulants (31). Briefly, in this method the correlation function is expanded in a power series. The expansion coefficients (cumulants) correspond to the moments of the intensity distribution. The first cumulant gives the mean ( $z$ -average) of the diffusion coefficient  $D$  and the second the variance (width) of its distribution. Thus for small particles in highly diluted solution the free particle translational diffusion coefficient  $D_0$ , which is related through the Stokes–Einstein equation  $D_0 = kT/6\pi\eta R_H$  to the hydrodynamic radius  $R_H$ , the size of an equivalent compact sphere, where  $k$  is the Boltzmann constant,  $T$  is the absolute temperature, and  $\eta$  is the viscosity of the solvent can be obtained. It is well known that the diffusion coefficient of particles in solution depends on the concentration due to interparticle interactions. These interactions lead to correlations in particle positions and motions. In a two-component system composed of rigid particles and liquid (32), three types of forces act on a particle: The first one is the Brownian force arising from collisions with thermally agitated liquid molecules. The second force arises from direct interactions between particles, which is, in the case of uncharged particles, a simple excluded volume or hard-sphere force. The third interaction is due to hydrodynamic interactions arising from the coupling between particle motions transmitted indirectly by the flows they induce in the liquid (32). This type of force becomes important for highly concentrated solutions. Because of this complex situation in nonideal solutions the measured diffusion coefficient is no longer the free particle diffusion coefficient  $D_0$  but is replaced by the so-called effective diffusion coefficient  $D_{\text{eff}}$  while the corresponding hydrodynamic radius is replaced by an apparent hydrodynamic radius  $R_{H,\text{app}}$ . Even though  $R_{H,\text{app}}$  is just proportional to the inverse of  $D_{\text{eff}}$ , it is helpful to determine both quantities.  $D_{\text{eff}}$  describes without any model the diffusion behavior while  $R_{H,\text{app}}$  gives at least a result in terms of a dimension that can be related directly to the SAS results.

In the so-called hydrodynamic regime  $q \ll q_m$ , where  $2\pi/q_m$  is the most probable interparticle spacing within the hard-sphere model we can use simple virial expansions to describe the concentration dependence of the effective diffusion coefficient  $D_{\text{eff}} = D_0(1 + 1.56\Phi)$  with  $\Phi$  being the volume fraction (32). This expression is, however, valid only in the case of low volume fractions and hard spheres. We are not aware of theoretical models that can describe the problem of diffusion hindrance of overlapping inverse micelles.

DLS measurements were carried out at a scattering angle of  $90^\circ$  and at a temperature of  $37^\circ\text{C}$ . The laboratory-built goniometer is equipped with an Argon ion laser (Spectra Physics, model Beamlok 2060A-5S,  $\lambda = 514.5 \text{ nm}$ ) and an ALV-5000E correlator (ALV, Langen, Germany). The effective power of

the primary beam was about 1 W. The intensity autocorrelation functions were analyzed using a second-order cumulant analysis (31), yielding an apparent diffusion coefficient  $D_{\text{eff}}$ . From  $D_{\text{eff}}$  the hydrodynamic radius  $R_{\text{H,app}}$  was calculated using  $R_{\text{H,app}} = k_B T / 6\pi\eta D_{\text{eff}}$ .

#### IV. RESULTS AND DISCUSSION

##### Small Angle X-ray Scattering (SAXS)

The investigated samples are in a concentration range from 5 up to 46 wt% SES surfactant for the pseudobinary systems. We have also investigated by SAXS the 30 wt% pseudobinary system with varying tetradecane to 1-butanol ratio (2 : 1, 1 : 1, and 1 : 2). For the pseudoternary systems up to 30% water are added to the 40 wt% pseudobinary solution (see Fig. 1). For the evaluation of such concentrated samples it is essential to take the effect of the interparticle interference into account. Therefore all measurements are evaluated with the GIFT method. For

both systems—the pseudobinary and the pseudoternary—it is necessary to mention that only the sugar headgroups of the SES molecules and, to a certain extent, the OH groups of the 1-butanol molecules associated with the micelles are visible in the SAXS measurements. The electron density of the solvent (tetradecane/1-butanol) is nearly the same as that for the long hydrocarbon chains of the surfactant. Therefore the maximum dimension visible in the PDDFs of the SAXS data are only related on the one hand to the hydrophilic sucrose groups for the pseudobinary samples and on the other hand to the sucrose groups with the water core for the pseudoternary systems.

*Pseudobinary system.* Figure 2A shows the experimental scattering curves of the pseudobinary system after subtraction of the blank scattering and the solvent. The interaction peak due to the increasing concentration is increasing significantly up to 40 wt% SES in solution. The samples with lower concentration show a very weak scattering signal due to the absence of fully developed globular micelles. This fact is also shown in Fig. 2B

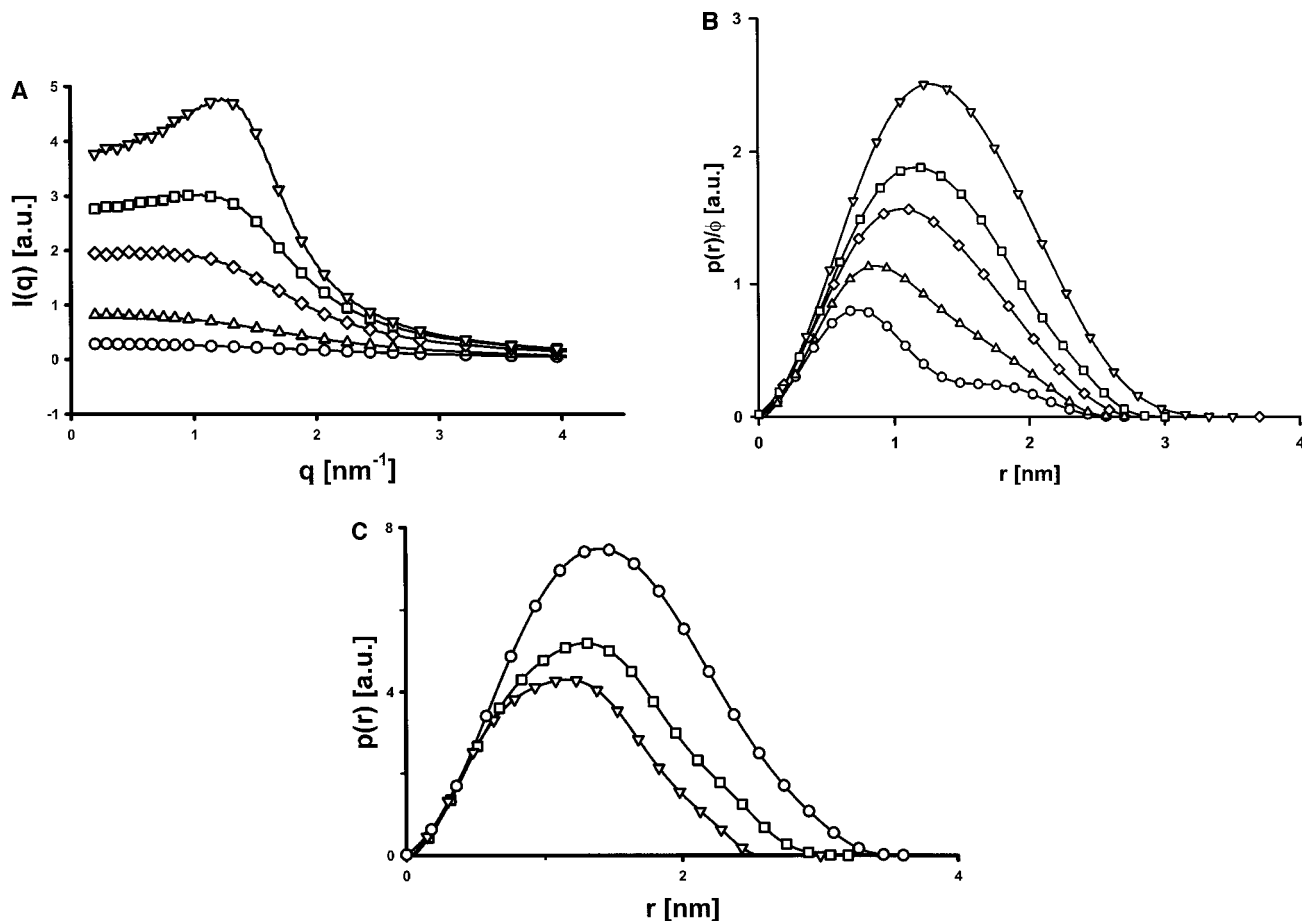


**FIG. 2.** (A) Experimental X-ray scattering curves after subtraction of the background and solvent scattering for the pseudobinary samples (SES in 1 : 1 tetradecane/1-butanol).  $\circ$ , 5%;  $\Delta$ , 10%;  $\diamond$ , 20%;  $\square$ , 30%;  $\nabla$ , 40% surfactant in the oil mixture. (B) The pair distance distribution functions (PDDFs) from the SAXS measurements; the height of the PDDFs is normalized by the volume fraction of the samples. Same symbols as in (A). (C) PDDFs of the 30 wt% SES sample with varying tetradecane to 1-butanol ratios:  $\circ$ , 2 : 1;  $\square$ , 1 : 1; and  $\nabla$ , 1 : 2. The area under the PDDF (aggregation number) increases with decreasing 1-butanol content.

where the corresponding pair distance distribution functions for the pseudobinary system are plotted for the whole concentration series normalized by the volume fraction of the samples. The area under the  $p(r)$  function is increasing with increasing concentration. The overall size of the inverse surfactant micelles increases only gradually with a maximal dimension of about 3 nm. Both facts together give the evidence that the aggregation number of the SES molecules in the micelles is growing with increasing surfactant concentration. Nothing can be said about the number of 1-butanol molecules in the micelles due to their negligible contribution to the scattering signal.

The  $p(r)$  functions for the solutions with lower concentration show a shape other than that of those with higher concentration. The PDDF for the 5 wt% solution shows a peak followed by a shoulder, which represents a mixture of monomers and oligomers of SES in the mixed micelles. The peak with a maximum at 1 nm can be related to very small structures like monomers, the shoulder to larger structures like oligomers, i.e., micelles with very low SES aggregation numbers, formed in this concentration range. These first micelles can be understood as aggregates, formed by only a few SES molecules and several 1-butanol molecules. Compared with the DLS measurements where the 5 wt% sample gives a very weak scattering signal, this is again a strong indication that the critical micellar concentration cmc is somewhere in the concentration range of about 5 to 10 wt%. The expression cmc is not perfectly correct in this situation. We use it for the concentration of SES, where the first mixed micelles with a measurable amount of SES molecules are formed. A similar wide concentration range for the building of micelles is known for other synthetic surfactants like triblock copolymers (Pluronic or Synperonic) (33). At higher concentrations 1-butanol is increasingly replaced by SES and globular micelles are formed in the samples. From 10 to 40 wt% the aggregation number increases by a factor of 4, the ratio is even higher for the 5 wt% solution, but could not be determined with reliable accuracy due to the low signal. No quantitative estimation of the aggregation numbers was possible as the data were not measured on absolute scale. Increasing the surfactant concentration toward the phase boundary (43 and 46 wt%) indicated a further increase of the aggregation number but did not show any drastic changes in the size or in the shape of the micelles (data not shown).

In order to investigate the replacement of 1-butanol by SES in detail, we studied the 30 wt% pseudobinary solution for three different compositions of the oil phase. We varied the ratio of tetradecane to 1-butanol from 1 : 2 to 1 : 1 and 2 : 1. The results are in full agreement with the above findings: the higher the ratio of SES to 1-butanol, the higher the SES aggregation number (area under the PDDF) and the larger the size of the micelles (see Fig. 2C). Taking the 1 : 1 mixture as a reference, the aggregation number decreases in the 1-butanol-rich sample (1 : 2) by 25% while it increases in the 1-butanol-lean sample (2 : 1) by more than 60%.

The different behavior of the systems with lower concentration (5 and 10 wt%) is visible in the phase diagram (Fig. 1). These

samples are not able to solubilize water in a sufficient amount. The forming of water-rich microemulsions is only possible with more than 20 wt% SES in the solution.

**Pseudoternary system.** In the following figures the SAXS scattering functions and PDDFs are shown for the pseudoternary system (microemulsions) with increasing water amount added to the pseudobinary sample with the highest concentration (40 wt% SES in the oil mixture). Figure 3A shows the experimental scattering curves for the pseudoternary system with interaction peaks shift to smaller  $q$  values with increasing water content, and Fig. 3B shows the corresponding PDDFs for the pseudoternary system. The  $p(r)$  functions show an increasing overall size with increasing water amount in the samples. The maximum dimension is increasing from 3 nm for the samples without water up to 6 nm for the sample with 30 wt% water added. In addition to this fact the shape of the micelles is also changing. The surfactant micelles without water are close to a compact globular structure but with increasing water amount the structure becomes more

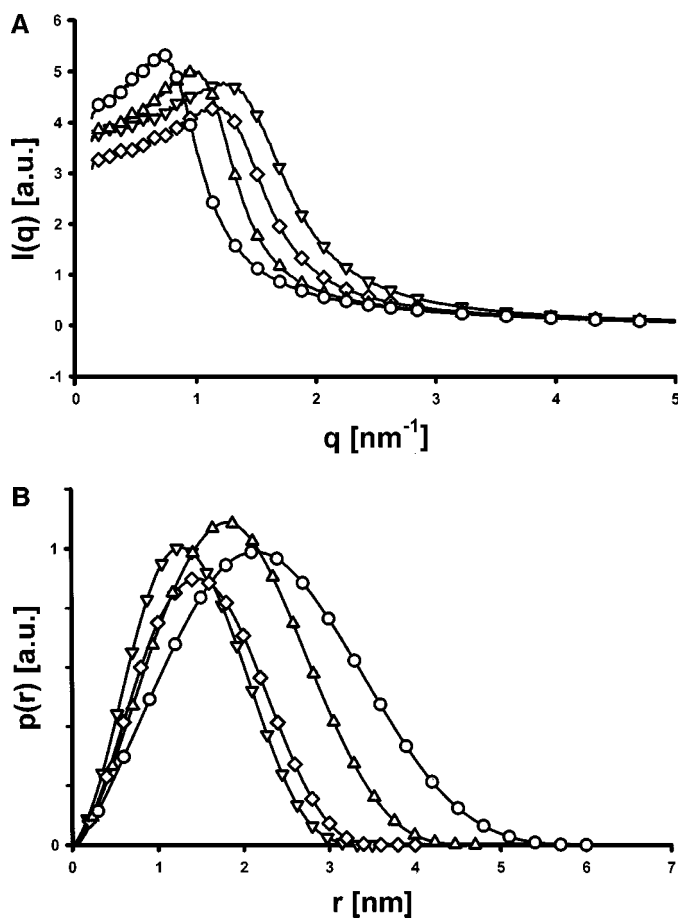


**FIG. 3.** (A) Experimental X-ray scattering curves for the pseudoternary system after subtraction of the background and solvent scattering, water added to the pseudobinary sample with highest concentration (40%).  $\nabla$ , 0% water added (40% pseudobinary sample);  $\diamond$ , 10% water added;  $\Delta$ , 20% water added;  $\circ$ , 30% water added. (B) The corresponding PDDFs for the pseudoternary systems.

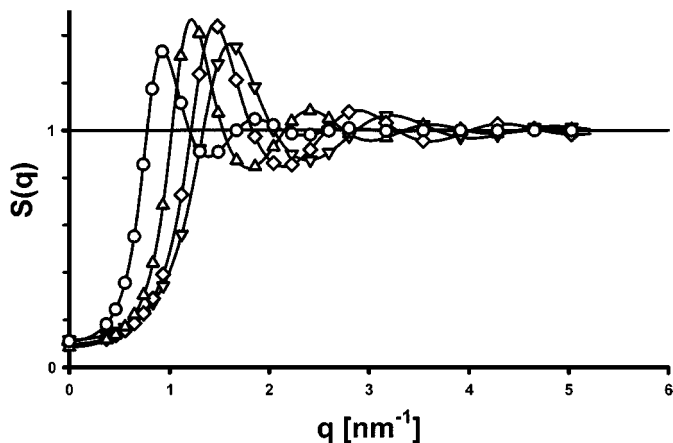


FIG. 4. The structure factors  $S(q)$  determined from the SAXS measurements shown in Fig. 3A.

and more elongated or polydisperse (this growth is documented by the increase of the ratio between maximum dimension to position of the maximum in  $p(r)$ ). It is not possible to distinguish between these two possibilities using only SAS data. The structure factors  $S(q)$  for the pseudoternary samples are shown in Fig. 4. The height of the oscillations is almost the same for all samples, but the position of the first maximum is shifted to smaller  $q$  values. This is also good evidence that the size of the particles in the samples is growing.

#### Small Angle Neutron Scattering (SANS)

In the following figures the same data as for SAXS are shown for the neutron scattering experiments. The solvent (tetradecane/*l*-butanol) and the water are fully deuterated, whereas the sucrose ester is protonated to get an adequate scattering contrast. The variation of the tetradecane to *l*-butanol mixing ratio was not measured by SANS. The data are evaluated like the SAXS data (GIFT).

**Pseudobinary system.** Figure 5A shows the experimental data of the SANS measurements with the best fit resulting from the application of the GIFT technique. The data for the samples with 10 and 20 wt% SES are not shown in the figure because of experimental problems during these measurements. In Fig. 5B the corresponding PDDFs are plotted normalized by the volume fraction of the samples. The overall size is again nearly the same for all pseudobinary solutions with a maximum dimension of about 6 nm. In the SANS data the whole surfactant molecule is visible because the sucrose ester is protonated and oil, *l*-butanol, and water are deuterated. Therefore the maximum dimensions for the particle size are larger than in SAXS where only the hydrophilic part is visible. Again it is evident that the sample with lower concentration gives a PDDF with a different shape. The same behavior was found for the SAXS data. This can be understood when considering that this sample is close to the cmc and the SES aggregation number is very low.

Again it is necessary to take the interparticle interaction into account. Although expecting that the inverse micelles interact rather like soft spheres than like hard spheres due to the hydrocarbon chains on the micellar surface we could use the evaluation technique GIFT, which models the interaction as polydisperse hard spheres. All data could be fitted within their error bands with this model. Taking into account the micellar size of about 6 nm, found from the form factor, it is however interesting to see that the hard-sphere interaction radius increases with concentration and is about 1.9 nm for the 40 wt% sample. The same interaction radius was found independently from the SAXS data, which is to be expected as the particle interaction and thus the mean spatial arrangement do not depend on the local contrast. This small interaction radius indicates an overlap of the outer part of the SES alkyl chains of neighboring inverse micelles. So we find a micellar diameter of about 6 nm, a center-to-center

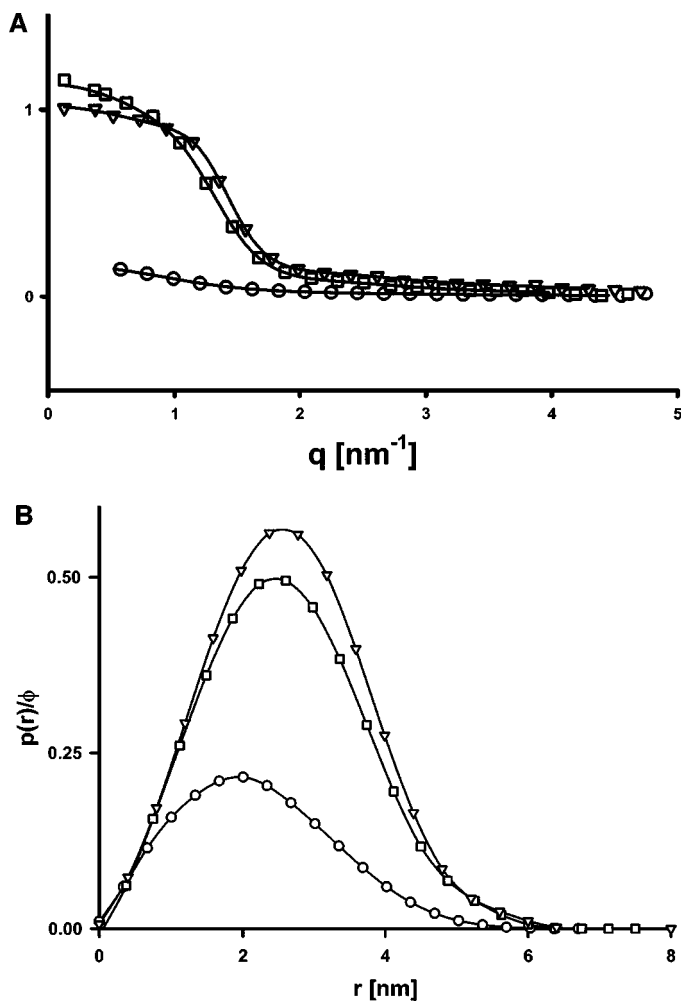
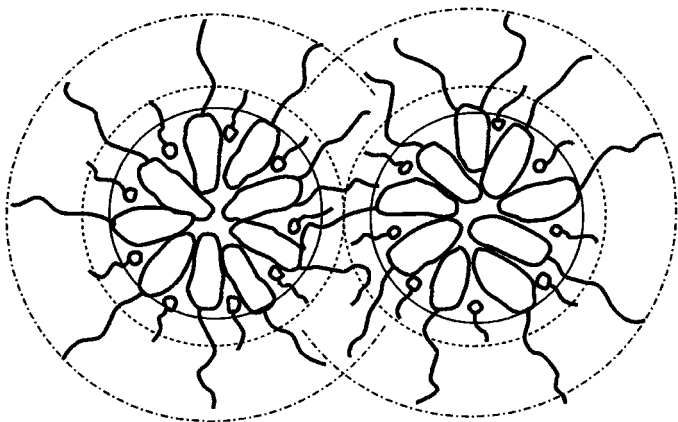


FIG. 5. (A) Experimental neutron scattering data for the pseudobinary systems (symbols:  $\circ$ , 5%;  $\square$ , 30%;  $\nabla$ , 40% surfactant in the oil mixture) and the best fit (full line). (B) The corresponding PDDFs for the pseudobinary systems from SANS measurements, where the height of the PDDFs is normalized by the volume fraction of the samples.



**FIG. 6.** Schematic model of the interacting micelles for the pseudobinary system at 40% SES concentration. Building elements are the SES and the BuOH molecules. The thin full line represents the core radius (headgroups), determined by SAXS, the dotted line the hard-sphere interaction radius, and the dashed-dotted line the overall radius determined by SANS.

distance (twice the interaction radius) of about 3.8 nm, and a headgroup diameter of about 3 nm. This situation is described qualitatively in Fig. 6 where the SES and BuOH molecules are depicted as building units together with the three different radii: the headgroup radius (determined by SAXS), the hard-sphere interaction radius (SAXS and SANS), and the radius of the micelles (SANS). The strong overlap is also manifested in their hydrodynamic behavior, i.e., reduced diffusion, found by the DLS measurements.

The picture of the micelles given in Fig. 6 is of course highly schematic. The effective radius of the headgroup area is clearly larger than their bare size. This is due to the fact that because the headgroups are not perfectly fixed in space, we measure a time-averaged distribution. A similar situation, i.e., a broadening of the headgroup area with a parallel decrease of the mean density, has also been found for micelles of the ganglioside GM3 (34).

*Pseudoternary system.* The  $p(r)$  functions for the pseudoternary systems (Fig. 7) show an increasing overall size with increasing water ( $D_2O$ ) amount. At the same time the overall contrast decreases for the samples with increasing water amount indicated by the decrease of the area under the  $p(r)$  function. The scattering length density difference of the protonated surfactant against the deuterated oil is negative, while  $D_2O$  is very close to the deuterated oil phase (see also the section Materials and Sample Preparation). So the addition of water leads to a situation of shell contrast. The maximum dimension is in the range of 6 nm for the water-free sample and up to 10 nm for the solution with 30 wt% water. The structure factors (not shown) present the same behavior as that for SAXS. The height of the oscillations is almost the same for all samples, but the position of the first maximum is shifted to smaller  $q$  values, which also indicates the particles are growing.

Again a structural change is found similar to the results of the SAXS measurements. The rather spherical shape of the

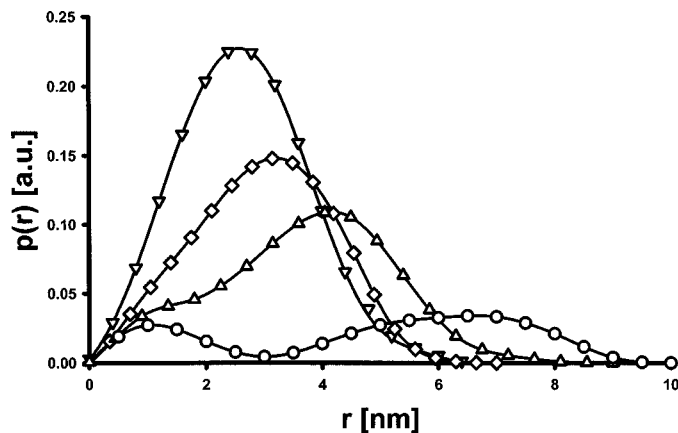


**FIG. 7.** The PPDFs from SANS measurements of the pseudoternary systems, where water ( $D_2O$ ) has been added to the pseudobinary sample with highest concentration (40%):  $\nabla$ , 0% water;  $\diamond$ , 10% water;  $\Delta$ , 20% water;  $\circ$ , 30% water added.

pseudobinary micelles becomes more elongated with increasing water amount.

One additional figure is shown for the neutron data. The PPDFs of the pseudoternary samples at lower water content are deconvoluted under the assumption of spherical symmetry to get the internal radial structure of the microemulsion. The averaged scattering length density profile across the microemulsion droplets was obtained by deconvolution of the PPDF. In Fig. 8 the deconvolution results for the 0% water sample (40 wt% pseudobinary sample) and for the samples with 10 and 20 wt% water are shown. The zero level is defined by the scattering length density of the deuterated oil mixture. The only uncertainty of this evaluation technique is the overall sign of the scattering length density profiles. This sign can be fixed, taking into account the fact that the protons of the surfactant molecules have a negative scattering length, whereas the deuterated water core has a positive one and is close to the deuterated oil phase. An

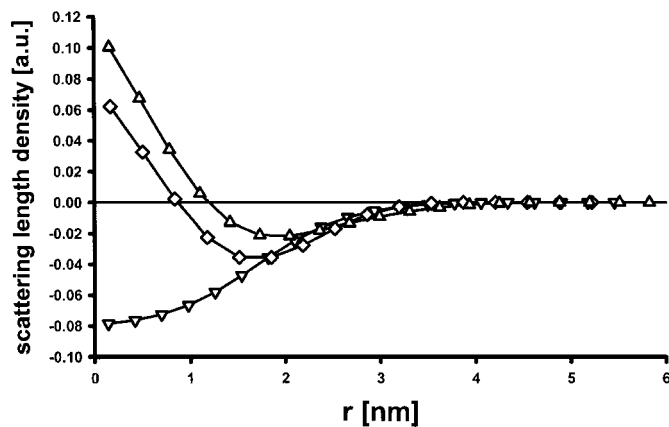


**FIG. 8.** The scattering length density profiles resulting from the deconvolution technique:  $\nabla$ , 0% water;  $\diamond$ , 10% water;  $\Delta$ , 20% water added.

ideal spherical shell would result in a triangularly shaped  $p(r)$  function.

This assignment of the overall sign is used in Fig. 8. The radius for the sugar-ester micelle is about 3 nm. For the samples with D<sub>2</sub>O added the inhomogeneity of the microemulsion becomes visible. The innermost part of the density profile is very poorly defined (resolution limit), but one can see that the negative part (SES shell) moves to higher  $r$  values with increasing water content. The zero crossing of the scattering length density distribution can be used to estimate the radius of the water core, which is in the range of about 1 nm. The width of the surfactant area is about 3 nm due to the size of the SES molecule. The scattering length density of the protonated surfactant molecules does not end in a sharp step function but is a slow approach to the background level because of the decaying radial density of the surfactant tails and due to the intercalation of the water molecules into the headgroup area. For the sample with the highest water content (30 wt%) the deconvolution does not work any more because the assumption of the spherical symmetry is no longer valid due to the elongation of the structures. Therefore no radial profile can be determined for this composition. This breakdown of the deconvolution technique is direct evidence of the nonsphericity of the particles.

#### Dynamic Light Scattering (DLS)

**Pseudobinary system.** DLS experiments were carried out for varying total concentrations ranging from 5 wt% surfactant up to 40 wt%. For the 5 wt% sample the intensity was extremely low (less than 30,000 counts/s at a laser power of 1 W). This signal led to a very poorly defined autocorrelation function that did not indicate the existence of SES micelles (results not shown). The contrast (ratio of refractive indices) of 1-butanol in tetradecane is too low to detect micelles without or with negligible SES content. The same holds for the SAS results, indicating that the cmc is located at relatively high concentrations of 5 to 10 wt%, as already discussed in the SAS section. The SAS results indicate mixed micelles are formed by only a few SES molecules together with some 1-butanol molecules. This can explain the low light scattering signal.

Starting with the 10 wt% sample we see an essential increase in the light scattering intensity, which levels off above 20 wt%. This increase is much stronger than to be expected for micelles growing only in number with concentration taking into account the excluded volume effect (see Fig. 9). This is in full agreement with the SES results showing an increase of the SES aggregation number in the micelles.

A strong decay of the effective diffusion coefficient measured with increasing surfactant concentration is observed (see Fig. 9). Based on the results of the SAS experiments we expect relatively small and globular micelles that hardly increase in size with increasing concentration. According to the diffusion coefficients measured with increasing concentration the apparent hydrodynamic radius  $R_{H,app}$  increases. For hard spheres one would expect a decrease of  $R_{H,app}$  following  $R_{H,app} \approx R_H/(1 + 1.56 \Phi)$ .

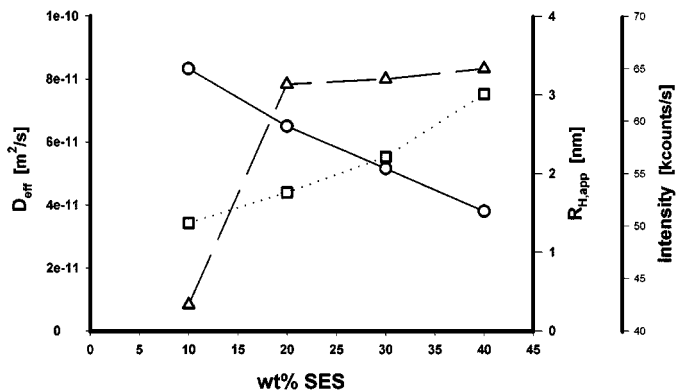


**FIG. 9.** DLS results for the pseudobinary system; the surfactant in 1-butanol/tetradecane (50/50 per wt). Shown are the effective diffusion coefficient  $D_{eff}$  (—○—), the apparent hydrodynamic radius  $R_{H,app}$  (··□··), and the integrated intensity (—△—) in arbitrary units as a function of the surfactant concentration. The connecting lines are shown as guides to the eye.

Qualitatively there are three possible situations that could explain the feature of decreasing  $D_{eff}$ : assuming repulsive excluded volume interactions, one must suggest strong concentration-induced micellar growth that more than compensates for the interaction effects, resulting in decreased  $D_{eff}$  values. However, as already mentioned above, SAS clearly indicates that the aggregates do not show micellar growth. The second possible explanation is attractive interaction for particles with  $c$ -independent size, which qualitatively would lead to a decrease of  $D_{eff}$  with increasing volume fraction. Looking at the corresponding static signal, the measured integrated intensity, one would indeed expect an increase due to the increasing concentration as well as due to attractive interaction effects. Both effects together should result in a very strong intensity increase. Instead of this expected behavior we observe only a very weak increase of the intensity at low volume fractions, which even reaches a plateau at higher concentrations. A value of 0.94 for the transmission of the highest concentration investigated ensures that multiple scattering can be neglected and is not the reason for the low intensities at higher concentrations. Anyway, also SAS experiments do not show any indication of attractive interactions between the micelles.

The third possible and most probable case is  $c$ -independent size, excluded volume effects arising from simple hard spheres interactions, and a change in the friction coefficient of the solution, which has consequences on the diffusion behavior. This scenario could qualitatively explain the weak concentration dependence of the integrated intensity. The radius of the particles determined with SAS is about 3 nm, while the calculated hard-sphere interaction radius is 1.9 nm both for SAXS and for SANS experiments. This indicates that the long alkyl chains of neighboring inverse micelles can overlap to a high degree without excluded volume effects (see Fig. 6). This strong overlapping must cause a steric hindrance and increasing friction, resulting in strongly decreasing values for  $D_{eff}$  while the mean spatial arrangement, determined by the SAS experiments, can still be

described excellently by excluded volume interaction. So we can understand from these results that there is a kind of dynamic entanglement of the interpenetrating micelles that leads to a slowing down of the diffusion but not to the formation of stable, large aggregates that would have been detected by the SAS experiments as well as by the integrated intensities of the DLS measurements.

Another point that we have neglected so far is the concentration-dependent partitioning of 1-butanol. 1-Butanol has also amphiphilic properties and will partly dissolve into the surfactant aggregates, which would result in a change of the solute away from the 1 : 1 1-butanol/tetradecane mixture as a function of surfactant concentration, which of course gives rise to different values for the viscosity and the refractive indexes. Thus obviously the unusual behavior of the DLS data cannot be understood with simple assumptions like hard-sphere interaction and can only be explained with the help of the SAS results, but there is finally no conflict between SAS and DLS data.

*Pseudoternary system.* Further DLS experiments were carried out for the 40 wt% surfactant sample with additional amounts of water, up to 30 wt%. Recalling the SAS experiments the static data show that the added water obviously partitions into the micelles, resulting in an increasing micellar size. Up to 20 wt% water the swollen micelles are approximately spherical. With 30 wt% water content the  $p(r)$  function indicates cylindrical rather than globular particle shape. In addition this is supported by the fact that the function cannot be deconvoluted any more.

Up to 20 wt% water DLS measurements show an increasing  $D_{\text{eff}}$  and slightly decreasing values for the corresponding intensities (Fig. 10). Simultaneously with the growth of the micelles the hydrophobic shell of the particles qualitatively changes due to the different curvature of the monolayer. The larger the particles, the lower the curvature and the more closely packed the hydrocarbon chains, which of course has its effect on the extent of the overlap of the hydrophobic regions between neighboring

particles. So with increasing swelling the mutual penetration of the hydrophobic regions by different micelles may decrease, resulting in a decreasing steric hindrance of the diffusive motion. This fact together with the hard-sphere interaction may explain the increase of  $D_{\text{eff}}$  with increasing water content despite slightly increasing micellar size. Between 20 and 30 wt% a change in the micellar shape from globular to cylindrical particles takes place, leading to even more complicated dynamic properties. We can observe a strong decay of the  $D_{\text{eff}}$  and at the same time a significant increase of the scattered intensity, both indicating micellar growth without a distinct modification of the friction compared to the 20 wt% solution due to only small changes in the curvature.

To summarize one can say that DLS is a fast method for obtaining information on the size of the particles in relatively simple and dilute systems, but in the case of the complex solutions investigated here it would not be possible to qualitatively interpret the respective results without the additional information from static experiments. So DLS and SAS are complementary techniques and the results support each other. Nevertheless, to extract quantitative information on dynamic measurements of such complex mixtures and to fully understand the results we would need much more a priori information on these systems.

## V. CONCLUSION

SAS methods are used to obtain valuable information about the size, shape, and internal structure of microemulsions, colloids, and microemulsions. For SAXS all components were used protonated because this technique depends on the difference of the electron density between particles and the surrounding media. The  $p(r)$  functions calculated from the SAXS data show continuous changes with concentration even though they are normalized to the volume fraction; i.e., if the aggregates would just increase in number but not change in composition or shape, the  $p(r)$  functions would be identical in this presentation. In reality we see two effects. At lower concentrations (5 and 10%) we see not only an increase in the area under this function, which corresponds to an increase of the SES aggregation number within the mixed SES-1-butanol micelles, but we see also a pronounced change in its shape, which indicates the transition from SES monomers or SES oligomers in the mixed micelles to micelles, where the SES molecules have such a high aggregation number that they are continuously distributed all over the surface of the globular micelles. This interpretation is also supported by the very low signal (scattering intensity) for these samples. The  $p(r)$  functions for concentrations between 20 and 40% have a very similar shape with the indication of a slight increase of the overall size, i.e., the micelles grow (increasing aggregation number), while remaining globular. These results can be understood as a concentration-dependent growth of the micelles, where especially the aggregation number of the SES molecules increases essentially. The dependence of this aggregation number on the relative amount of SES vs 1-butanol was

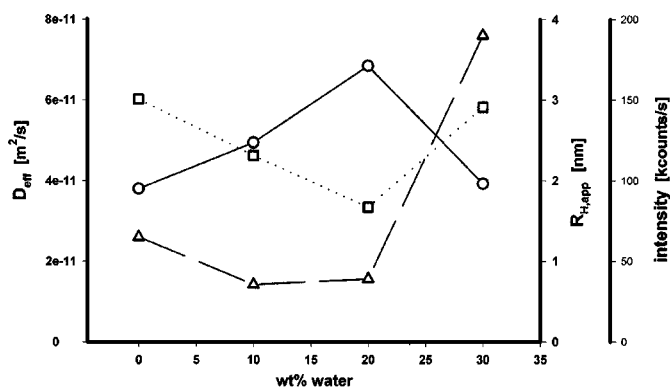


**FIG. 10.** DLS results for the 40 wt% surfactant in the 1-butanol/tetradecane (50/50 per wt) sample with different amounts of water; shown are the effective diffusion coefficient  $D_{\text{eff}}$  (—○—), the apparent hydrodynamic radius  $R_{\text{H,app}}$  (··□··), and the integrated intensity (—△—) in arbitrary units. The connecting lines are shown as guides to the eye.

cross-checked by a variation of the tetradecane to 1-butanol ratio from 2 : 1 to 1 : 2 at a fixed SES concentration of 30 wt%.

Adding water to the pseudobinary system caused the micelles to start swelling. The overall size of the micelles increases with increasing water amount. The micelles incorporate water inside the micellar core and form microemulsions. For SAXS measurements only the polar headgroups and the water core are visible because of the similarity of the electron density of the hydrocarbon chains of the surfactant and the oil phase. Therefore the micelles seem to be rather small due to the invisible hydrophobic part of the SES.

For SANS experiments the solvents used are deuterated and the surfactant is protonated to get high scattering contrast. Therefore the whole protonated micelles (heads and hydrocarbon chains) are visible and the overall size appears to be larger than that for SAXS experiments. The characteristics investigated are analogous to the SAXS results. The radius of the particles is about 3 nm, while the calculated hard-sphere interaction radius is 1.9 nm nearly for the 40 wt% pseudobinary sample like in the case of SAXS. This indicates that the long alkyl chains of neighboring micelles can overlap to a high degree without excluded volume effect. For the SANS measurements an additional evaluation step was possible. The PDDFs of the pseudoternary samples are deconvoluted under the assumption of spherical symmetry to get the internal structure of the microemulsion. The radius of the water-free surfactant micelles is about 3 nm. When adding water to the pseudobinary system the incorporated water core can be estimated with a radius of about 1 nm. The width of the surfactant layer remains about 3 nm due to the size of the SES molecule. The measured dynamic behavior of these systems show a steric hindrance caused by the strong overlapping of these inverse micelles due to the high concentrations. As already mentioned, we were able to fit all our SAS data within their statistical accuracy by a hard-sphere interaction model, but we must admit that we cannot exclude a very weak attractive interaction. However, essential attractive contributions would lead to conflicting results for the effective volume fraction in the hard-sphere approximation, which were not found in our experiments.

Finally it is to mention that such systems are rather difficult to handle due to the characteristic phase behavior (demixing at lower temperatures). Their scattering data are not easy to evaluate because these systems contain four components in different ratios. To summarize one can say that SAS and DLS are useful complementary techniques for getting qualitative and quantitative information about such complex systems.

#### ACKNOWLEDGMENTS

The SANS results report were obtained in Experiments 9-10-420 at the Institute Laue Langevin (ILL) in Grenoble, France. We thank our local contact, Roland May, for all his help and patience during our experiments at D22. We

are grateful for the support by Research Grant P11778-CHE from the Austrian "Fonds zur Förderung der wissenschaftlichen Forschung."

#### REFERENCES

1. Strey, R., and Jonstromer, M., *J. Phys. Chem.* **96**, 4573 (1992).
2. Bansal, V. K., Shah, D. O., and O'Connell, J. P., *J. Colloid Interface Sci.* **75**, 462 (1980).
3. Shinoda, K., and Shibata, Y., *Colloids Surf.* **19**, 185 (1986).
4. Kahlweit, M., Strey, R., and Busse, J., *J. Phys. Chem.* **94**, 3881 (1990).
5. Paul, B. K., and Moulik, S. K., *J. Dispers. Sci. Technol.* **18**, 301 (1997).
6. Kunieda, H., and Yamagata, M., *Langmuir* **9**, 3345 (1993).
7. Garti, N., Aserin, A., Ezrahi, S., and Wachtel, E., *J. Colloid Interface Sci.* **178**, 60 (1996).
8. Kunieda, H., Ushio, N., Nakano, A., and Miura, M., *J. Colloid Interface Sci.* **159**, 37 (1993).
9. Thevenin, M. A., Grossiord, J. L., and Poelman, M. C., *Int. J. Pharm.* **137**, 177 (1996).
10. Bolzinger-Thevenin, M. A., Grossiord, J. L., and Poelman, M. C., *Int. J. Pharm.* **176**, 39 (1998). Bolzinger-Thevenin, M. A., Grossiord, J. L., and Poelman, M. C., *Langmuir* **15**, 2307 (1999).
11. Aramaki, K., Kunieda, H., Ishitobi, M., and Tagawa, T., *Langmuir* **13**, 2266 (1997).
12. Pes, M. A., Aramaki, K., Nakamura, N., and Kunieda, H., *J. Colloid Interface Sci.* **178**, 666 (1996).
13. Kawaguchi, T., Hamanaka, T., Kito, Y., and Machida, H., *J. Phys. Chem.* **95**, 3837 (1991).
14. Garti, N., Aserin, A., Leser, M. E., Clement, V., and Fanun, M., *J. Mol. Liquids* **80**, 253 (1999). Garti, N., Clément, V., Fanun, M., and Leser, M. E., *J. Agric. Food Chem.* **48**, 3945 (2000).
15. Fanun, M., Wachtel, Antelek, B., Aserin, A., and Garti, N., *Colloids Surf. A: Physicochem. Eng. Aspects* **180**, 173 (2000).
16. Glatter, O., Strey, R., Schubert, K.-V., and Kaler, E. W., *Ber. Bunsenges. Phys. Chem.* **100**, 323 (1996).
17. Iampietro, D. I., Brasher, L. L., Kaler, E. W., Stradner, A., and Glatter, O., *J. Phys. Chem. B* **102**, 3105 (1998).
18. Glatter, O., *J. Appl. Cryst.* **10**, 415 (1977).
19. Glatter, O., in "Small Angle X-ray Scattering" (O. Glatter and O. Kratky, Eds.), p. 119. Academic Press, London, 1982.
20. Glatter, O., *J. Appl. Cryst.* **14**, 101 (1981).
21. Glatter, O., and Hainisch, B., *J. Appl. Cryst.* **17**, 435 (1984).
22. Glatter, O., *Prog. Colloid Polym. Sci.* **84**, 46 (1991).
23. Mittelbach, R., and Glatter, O., *J. Appl. Cryst.* **31**, 600 (1998).
24. Brunner-Popela, J., and Glatter, O., *J. Appl. Cryst.* **30**, 431 (1997).
25. Weyerich, B., Brunner-Popela, J., and Glatter, O., *J. Appl. Cryst.* **32**, 197 (1999).
26. Brunner-Popela, J., Mittelbach, R., Strey, R., Schubert, K.-V., Kaler, E. W. and Glatter, O., *J. Chem. Phys.* **21**, 10,623 (1999).
27. Bergmann, A., Fritz, G., and Glatter, O., *J. Appl. Cryst.* **33**, 1212 (2000).
28. Glatter, O., Fritz, G., Lindner, H., Brunner-Popela, J., Mittelbach, R., Strey, R., Stefan, U., and Egelhaaf, S. U., *Langmuir* **16**, 8692 (2000).
29. Fritz, G., Bergmann, A., and Glatter, O., *J. Chem. Phys.* **113**, 9733 (2000).
30. Bergmann, A., Orthaber, D., Scherf, G., and Glatter, O., *J. Appl. Cryst.* **33**, 869 (2000).
31. Koppel, D. E., *J. Chem. Phys.* **57**, 4814 (1972).
32. Pusey, P., and Tough, R. J. A., in "Dynamic Light Scattering" (R. Pecora, Ed.), p. 85. Plenum Press, New York, 1985.
33. Glatter, O., Scherf, G., Schillén, K., and Brown, W., *Macromolecules* **27**, 6046 (1994).
34. Maurer, N., Cantù, L., and Glatter, O., *Chem. Phys. Lipids* **78**, 47 (1995).